Applied Surface Science 458 (2018) 397–404

Contents lists available at ScienceDirect

Applied Surface Science

journal homepage: www.elsevier.com/locate/apsusc

Full Length Article

Promoted methane activation on doped ceria via occupation of Pr(4f) states

Agustín Salcedo, Ignacio Iglesias, Fernando Mariño, Beatriz Irigoyen*

Universidad de Buenos Aires, Facultad de Ingeniería, Departamento de Ingeniería Química, Pabellón de Industrias, Ciudad Universitaria, C1428EGA Buenos Aires, Argentina

CONICET–Universidad de Buenos Aires, Instituto de Tecnologías del Hidrógeno y Energías Sostenibles (ITHES), Pabellón de Industrias, Ciudad Universitaria, C1428EGA Buenos Aires, Argentina

ARTICLE INFO

Keywords:
Methane activation
Pr-doped ceria
DFT
Hydrogen

ABSTRACT

Steam reforming of the methane stream obtained from biomass gasification is a potential route for sustainable syngas (CO + H_2) and hydrogen production. The rate-limiting step for the reactions involved in methane steam reforming (MSR) is thought to be CH_4 activation. Praseodymium-doped ceria-based catalysts, with easily reducible Pr cations and high oxygen storage capacity, could be attractive for MSR. In this work, we performed density functional theory (DFT) calculations to examine the activity of a low Pr-doped CeO_2(1 1 1) surface for methane reforming. The results show a significant lowering (0.48 eV) of the energy barrier for methane activation via homolytic H_3C—H bond cleavage. This can be mainly explained by the easy occupation of Pr(4f) gap states by electrons transferred from adsorbed hydrogen species. The promotion of methane activation upon Pr doping of ceria was corroborated with methane temperature-programed reduction (CH_4-TPR) experiments conducted in both $Ce_{0.95}Pr_{0.05}O_2$ and CeO_2 samples.

1. Introduction

Global energy consumption has firmly increased during the last decades. Much of this growth has been satisfied with fossil resources, which leads not only to their depletion but also to environmental pollution. Concerns about petroleum and natural gas exhaustion, and greenhouse effect due to carbon dioxide emissions, have motivated the research of non-fossil renewable energy sources. Among them, hydrogen (H_2), as an energy carrier, is considered one of the most promising unconventional fuels. Hydrogen is capable of driving electricity generation without emission of harmful pollutants, which makes it an attractive fuel for powering vehicles, among other applications [1–3]. Furthermore, hydrogen has a high-energy yield of 122 kJ/g, which is 2.75 times greater than hydrocarbon fuels [3].

Biomass gasification is a valuable alternative for sustainable hydrogen production. At present, H_2 is mostly obtained from fossil resources. Using biomass instead of fossil fuels reduces environmental pollution, since the carbon dioxide released as a by-product of biomass gasification was previously absorbed from the atmosphere and fixed by photosynthesis in the growing biomass [4]. The main products of biomass gasification are methane (CH_4), hydrogen and carbon monoxide (CO). Carbon dioxide (CO_2), light hydrocarbons and sulfur compounds [5] are also produced. This stream can be transformed into syngas (a mixture of CO and H_2) and improved in its H_2 content by catalytic reforming of methane.

The methane steam reforming (MSR) process is an efficient and well-established method to produce hydrogen, which involves two main reactions: (i) the endothermic generation of syngas from methane, and (ii) the exothermic water-gas shift (WGS) reaction that transforms CO into more H_2. Overall, the MSR process is endothermic and high-energy demanding, and therefore it is usually carried out at high temperatures (> 700 °C), which results in reduced efficiency and elevated costs. Hence, the development of a selective and sulfur-tolerant catalytic system to convert biomass-derived methane into hydrogen at low temperatures is a major technological challenge.

Considerable work has been done to develop a suitable catalyst for methane steam reforming. Among the many metals that can be used as an active phase (Ni, Ru, Rh, Pd, Ir, Pt), nickel is one of the preferred, mainly due to its high reactivity and low cost [6,7]. Ni supported on alumina (Al_2O_3) are widely used as a catalyst in industrial processes [8]. Ni/α-Al_2O_3 catalysts have been traditionally used to produce syngas from methane steam reforming because of their superior thermal and mechanical stability [8]. Despite their high activity and low cost, these catalysts are frequently deactivated by coking, sulfur poisoning and nickel sintering [9].

Several alternative supports (ZrO_2, $MgAl_2O_4$, CaO, CeO_2) have been

* Corresponding author at: Universidad de Buenos Aires, Facultad de Ingeniería, Departamento de Ingeniería Química, Pabellón de Industrias, Ciudad Universitaria, C1428EGA Buenos Aires, Argentina.
E-mail address: beatriz@di.fcen.uba.ar (B. Irigoyen).

https://doi.org/10.1016/j.apsusc.2018.07.090
Received 9 April 2018; Received in revised form 19 June 2018; Accepted 11 July 2018

proposed to overcome these disadvantages [10]. Among them, cerium oxide (CeO_2, ceria) is especially interesting due to its high oxygen storage capacity (OSC); which plays a key role in improving the resistance of Ni-based catalysts to deactivation by coke deposition, allowing rapid CH_x oxidation and CO or CO_2 release to the gas phase depending on experimental conditions [11–14]. Indeed, experimental results have shown that below 810 °C the CO_2 formation rate is higher than that of CO, with the latter being practically zero below 700 °C [14]. This feature is mainly attributed to oxygen donation from the ceria support, essentially because Ce cations can undergo rapid redox (Ce^{4+}/Ce^{3+}) cycles [15–17].

Many experimental works have indicated that a metallic active phase (usually nickel) is needed to achieve satisfactory catalytic performance for the MSR reactions [17]. Notwithstanding, it has been proposed that reforming reactions involve methane and CH_x species interacting with surface oxygen on the metal-oxide support via a Mars–van Krevelen mechanism [18–20]. Overall, the exact mechanisms implicated in methane dehydrogenation and oxidation reactions are still under discussion. Nonetheless, a reducible support such as CeO_2 has desirable characteristics like its high OSC and oxygen mobility and should play a key role in MSR reactions.

Cerium oxide can be doped with transition, alkaline or rare earths metals to improve its oxygen storage capacity, redox properties, thermal stability and oxygen mobility [21,22].

Improved OSC has been reported after partial substitution of cerium with unreducible dopants, which is attributed to the difference in their ionic radius [23]. In this sense, doping CeO_2 with metal cations of ionic radius lower than that of Ce^{4+} is accepted to increase ceria reducibility by introducing distortions of the fluorite structure [24,25]. For instance, Zr addition to CeO_2 leads to CeO_2–ZrO_2 solid solutions with high OSC and improved catalytic activity under both oxidizing and reducing conditions [21,25,26].

On the other hand, higher OSC has also been attained after cerium partial substitution by a reducible dopant of ionic radius like that of Ce^{4+}, like praseodymium (Pr). Praseodymium doping of CeO_2 does not significantly distort the crystal structure, but it enhances the formation and migration of oxygen vacancies, achieving an OSC comparable to that of CeO_2–ZrO_2 materials [27–29]. Furthermore, first principle calculations performed on the Pr-doped CeO_2(1 1 1) surface show that the energy required to form an oxygen vacancy is lower than in pure ceria [30–32].

Concerning the catalytic performance of Pr-doped ceria, it is worth noting that samples prepared in our laboratory with low content of Pr (~5 at%) have shown superior activity for CO preferential oxidation and WGS reactions [30,31]. This improvement has been attributed to easy formation of Pr^{3+}/Pr^{4+} redox couples [32,33]. Besides, Pr doping also appears to enhance the catalytic performance of ceria for methane reforming in the presence of H_2S, mainly due to formation of surface oxysulfide species [34].

The superior catalytic performance of Pr-doped CeO_2 solid solutions in oxidation reactions allows us to anticipate a promising behavior of these solids as supports of a Ni active phase for the MSR process. Therefore, in the present work we examined CH_4 interactions on the $Ce_{0.963}Pr_{0.037}O_2$(1 1 1) surface using density functional theory (DFT) calculations. We computed adsorption energies, activation barriers, geometric and electronic structures, and electron transfer between adsorbates and the surface. Our theoretical findings were validated against experimental temperature-programmed reduction with methane (CH_4-TPR) measurements.

2. Methodology

2.1. Computational details and surface models

First principles calculations were performed within the spin-polarized density functional theory (DFT) framework as implemented in the Vienna Ab-initio Simulation Package (VASP) [35,36]. Adsorbate and surface geometries were optimized until the Hellmann–Feynman forces converged to less than 0.02 eV/Å. The Kohn–Sham equations were solved within the generalized gradient approximation (GGA), with the exchange-correlation functional of Perdew–Burke–Ernzerhof (PBE) [37]. We treated explicitly the Ce($5s^25p^66s^25d^14f^1$), Pr ($5s^25p^66s^25d^14f^2$), O($2s^22p^4$), C($2s^22p^2$) and H($1s^1$) valence electrons in a plane wave basis with a cutoff energy of 480 eV, whereas the remaining electrons were represented with the projector-augmented wave (PAW) method [38,39]. Self-consistent calculations were performed sampling the Brillouin zone with a 3 × 3 × 1 k–point mesh under the Monkhorst–Pack scheme [40].

Standard DFT is unsuccessful in describing strongly correlated electrons in partially occupied d and f orbitals because it underestimates on-site Coulomb repulsions [41–45]. A better description is provided by the DFT + U method, where the introduction of a Hubbard parameter U compensates the electron self-interaction error and enhances the description of the correlation effects. In Dudarev's formalism [46] the Coulomb repulsion parameter U and exchange interaction parameter J enter as a single parameter $U_{eff} = U - J$. For Ce(4f) states, the value $U_{eff} = 5$ eV was chosen because it correctly described the atomic and electronic structure of both CeO_2 and CeO_{2-x} systems [41,47–49]. For Pr(4f) states, the value $U_{eff} = 4.5$ eV has reproduced the available experimental data for PrO_2 such as lattice constant and band gap [24].

DFT + U calculations do not account properly for van der Waals (vdW) dispersion forces, which might play some role in stabilizing weak adsorbate-surface interactions. Due to the importance of these interactions, a lot of effort has been directed in the last years to develop ways to correctly describe vdW forces within a DFT approach, and a variety of methods have been proposed. In this work, we employed the nonlocal vdW-DF functional of Langreth and Lundqvist et al. [50], which has been previously applied to cerium oxide [51]. Specifically, we used the alternative exchange functional optB86b as implemented in VASP [52,53].

To identify the transition state (TS) structures we employed the climbing image nudged elastic band method (CI-NEB) [54], with the images optimized while constrained along the reaction coordinate. The harmonic vibrational modes were calculated to confirm a single imaginary frequency.

Oxidation states, electron occupancy and spin charge density were calculated using Bader's atom in molecules approach [55,56].

Cerium oxide (CeO_2) crystalizes in a fluorite-type structure, a face-centered cubic (fcc) lattice of Ce^{4+} cations with O^{2-} anions filling the tetrahedral voids. The reported experimental lattice parameter of CeO_2 is 5.41 Å [57]. Ce partial substitution by Pr leads to formation of solid solutions [58–60]. This process is facilitated by the similarity of Ce^{4+} and Pr^{4+} ionic radius (0.96 Å and 0.97 Å, respectively [61]). Successful Pr incorporation into the CeO_2 lattice has been confirmed by X-ray diffraction (XRD) studies [59]. For a Pr content of 5 at%, Rietveld analysis of the XRD diffraction pattern resulted in a lattice parameter of 5.44 Å [31]; which is about 0.6% higher than the value of 5.41 Å reported for the bulk structure of bare ceria.

The CeO_2 surface was obtained by cleaving the bulk fluorite-type structure with the (1 1 1) plane and retaining an extra oxygen layer. The (1 1 1) plane is the most stable among the low-index (1 1 1), (1 1 0) and (1 0 0), and corresponds to minimal Ce—O bonds cleavage [62–64]. Considering the theoretical and experimental information available, we modeled the CeO_2(1 1 1) surface in a p(3 × 3) slab with 9 atomic layers and an empty space of 18 Å (Fig. 1a). The empty space avoids periodic interactions with the atoms of the upper image. Next, a Pr-doped CeO_2(1 1 1) surface was built by substituting one surface Ce cation by Pr in the p(3 × 3) slab [32]. This way, a Pr content of 3.7 at% was achieved. The resulting $Ce_{0.963}Pr_{0.037}O_2$(1 1 1) surface is shown in Fig. 1b. For both surfaces, full relaxation of atomic coordinates was allowed for the ions located in the six uppermost slab layers, while the

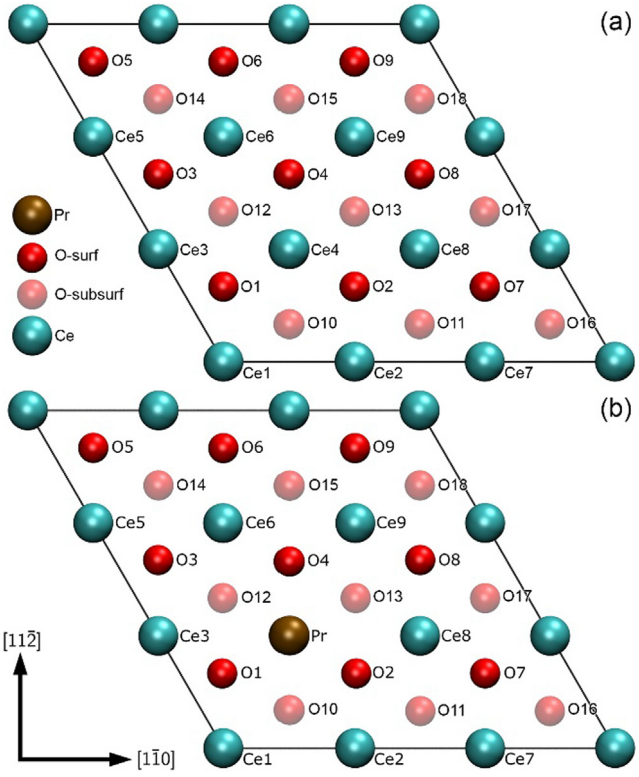

Fig. 1. (a) CeO_2(1 1 1) slab. (b) $Ce_{0.963}Pr_{0.037}O_2$(1 1 1) slab.

ions in the three bottom layers where kept fixed in their bulk positions.

2.2. Experimental

Praseodymium-doped ceria sample was prepared by coprecipitation using the urea thermal decomposition method, a highly reproducible synthesis method for ceria-based materials as shown in a previous work by our group [65]. Atomic percentage of praseodymium in the Pr-doped sample was 5%. Aqueous solutions of urea, ceria and praseodymium nitrates were prepared with a 10:1 urea-cations ratio and kept at 90 °C for 24 h. The precipitate obtained was washed and centrifuged three times before drying at 80 °C overnight. Afterwards, the solid was calcined for 5 h in muffle at 900 °C.

Temperature programmed reduction with methane (CH_4-TPR) and oxygen storage capacity (OSC) experiments were conducted in a quartz fixed bed reactor with a Micromeritics AutoChem II apparatus. Gases from the reactor were analyzed with a Pfeiffer Omnistar quadrupolar mass spectrometer. Mass flow controllers contained in the AutoChem II were calibrated for the gases used in the experiments and the Pfeiffer Omnistar quadrupolar mass spectrometer was regularly calibrated as well. For CH_4-TPR experiments, mass employed was 50 mg and total gas flow was 50 Nml/min (5% CH_4/Ar), and temperature was raised from 500 to 600 °C (10 °C/min). Before reduction, Pr-doped and undoped ceria samples were treated under air flow at 450 °C for 1 h to ensure surfaces cleanliness, since they are prone to adsorb impurities, mainly carbonates [66]. This temperature was found to be adequate to eliminate carbonates in the samples, irrespective of the calcination temperature selected for CH_4-TPR and OSC experiments. For OSC measurements at isothermal conditions (400 °C), we followed the traditional method described by Yao and YuYao [67]. Alternating pulses of oxidant (air) and reductant (5% CO/Ar) were injected until stable CO_2 production was registered (OSC). A more detailed description and characterization of samples is available in a previous work [68].

3. Results and discussion

In Section 3.1, we discuss our DFT calculations for methane interactions with the stoichiometric CeO_2(1 1 1) and $Ce_{0.963}Pr_{0.037}O_2$(1 1 1) surfaces. We report adsorption and activation energies, and examine density of states and Bader charges to identify reduced ions and oxidation states. Next, in Section 3.2, we study the behavior of reduced Pr^{3+} cations, by exploring the methyl adsorption step and methane interactions with a non-stoichiometric $Ce_{0.963}Pr_{0.037}O_{2-x}$(1 1 1) surface. Finally, we discuss our CH_4-TPR results for CeO_2 and $Ce_{0.95}Pr_{0.05}O_2$ samples in Section 3.3.

3.1. Methane interactions on stoichiometric surfaces

First, we evaluated methane molecular adsorption on top of each potential active site of the CeO_2(1 1 1) and $Ce_{0.963}Pr_{0.037}O_2$(1 1 1) surfaces. For all studied configurations, the adsorption energy of a CH_4 molecule was calculated as:

$$\Delta E\,[\mathrm{ads,CH_4}] \;= E\,[\mathrm{CH_4^*}] - E\,[\mathrm{CH_4}] - E\,[\mathrm{surface}]$$

In this formula, E[CH_4*] is the computed total energy of the surface slab with CH_4 on top of an ion, E[surface] is the energy of the clean surface and E[CH_4] is the energy of an isolated CH_4 molecule.

In the stoichiometric CeO_2(1 1 1) surface, the arrangement of cerium cations and oxygen anions is regular and symmetric (see Fig. 1a). The potential active sites are a Ce cation, a surface oxygen anion, and a subsurface oxygen anion. Computation of methane interactions on these sites resulted in adsorption energies close to zero (~0.01 eV), in good agreement with other reported theoretical results [69,70]. In all cases, the CH_4 molecule remains floating above the CeO_2(1 1 1) surface, located no less than 2 Å away from the oxygen layer. Surface ions do not show significant relaxation.

Concerning the $Ce_{0.963}Pr_{0.037}O_2$(1 1 1) surface, we differentiate nine possible active sites by their distance to the Pr dopant (see Fig. 1b): two Ce cations (Ce1 and Ce7), three surface O anions (O8, O6 and O4), three subsurface O anions (O11, O12 and O14), and the Pr cation itself. We studied methane interactions on each of these nine different sites. In all cases the calculated interaction energy (~0.01 eV) was like that computed for the undoped surface, which means that the methane molecule adsorbs weakly on both surfaces.

Next, we evaluated methane activation on the CeO_2(1 1 1) and $Ce_{0.963}Pr_{0.037}O_2$(1 1 1) surfaces. Methane C—H bonds are very stable (Δ_dH = 440 kJ/mol) and only weakly polarized, which makes the first C—H bond cleavage a difficult reaction step [71]. Knapp and Ziegler studied methane activation on the CeO_2(1 1 1) surface [19], and evaluated both simultaneous formation of C—O and H—O bonds on adjacent surface oxygen atoms and a rebound mechanism. The latter, in which a methyl radical is released to gas phase leaving behind a hydrogen atom adsorbed on the surface, was reported to be the most efficient, with an energy barrier of 1.44 eV.

Thus, we computed the total energy of a system consisting of hydrogen adsorbed on an oxygen anion (O4) and CH_3 floating on top of the surface. We indicate this configuration as pseudo-transition state (pTS) following the notation proposed by the Janik group [69]. The pTS is not a true transition state in that it has no imaginary frequency, but it is a high-energy intermediate between dissociative adsorption –with both methyl and hydrogen adsorbed on the surface– and molecular adsorption.

The energy for this reaction step was calculated as follows:

$$\Delta E\,[\mathrm{pTS}] \;= E\,[\mathrm{pTS}] - E\,[\mathrm{CH_4}] - E\,[\mathrm{surface}]$$

Concerning the CeO_2(1 1 1) surface, we computed an endothermic energy of 1.01 eV for the pTS. We also located the true transition state (TS) by CI-NEB sampling, in which the methyl is closer to the surface, and the hydrogen interacts with both methyl and a surface oxygen atom. These calculations indicate that methane first dissociation is

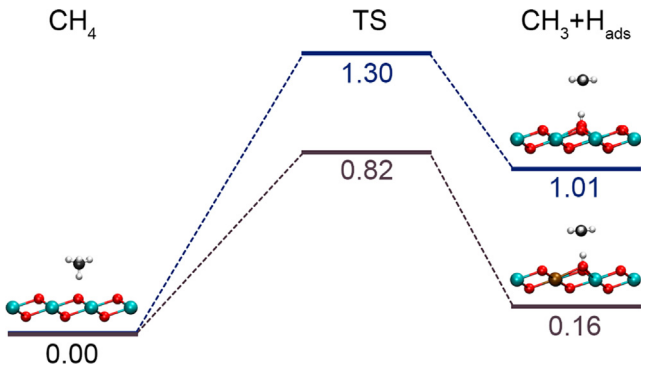

Fig. 2. Reaction coordinate diagram for the pseudo-transition state formation on both the undoped surface (blue) and the doped surface (brown). Values in electronvolt (eV).

hindered by an activation energy of 1.30 eV in the CeO_2(1 1 1) surface.

On the other hand, for the pseudo-transition state in the $Ce_{0.963}Pr_{0.037}O_2$(1 1 1) surface we computed an energy of 0.16 eV, which means that dissociation on this surface is more stable than on the undoped CeO_2(1 1 1) surface by 0.85 eV. The energy barrier is also lowered by 0.48 eV compared to the value computed on undoped ceria. Furthermore, pTS on the Pr-doped surface is only 0.16 eV less stable than molecular adsorption on the O4 site, indicating that Pr doping could promote activation of the CH_4 molecule. Fig. 2, summarizes these results in a reaction coordinate diagram.

Regarding pTS and surface atomic relaxation, hydrogen adsorbs on top of O4 forming a H—O4 bond of 0.98 Å in length while the O4 anion ascends 0.36 Å. Also, the nearest neighbor cations Ce6 and Ce9 are drawn away 0.12 Å from their original positions, increasing their Ce—O bond length to 2.61 Å. This means that the H—O4 bond formation pulls O4 away from the surface, weakening the Ce—O4 bond. The length of the Pr—O bonds with the nearest neighbors O1 and O2 is increased by 0.16 Å. Besides, CH_3 distance to the adsorbed H is 2.15 Å in $Ce_{0.963}Pr_{0.037}O_2$(1 1 1) and 2.99 Å in CeO_2(1 1 1); thus, confirming a C—H bond cleavage in the pTS for both surfaces.

The configuration of TS is different depending on solids. For CeO_2(1 1 1), the H is adsorbed on a surface oxygen and CH_3 adopts its planar geometry. For $Ce_{0.963}Pr_{0.037}O_2$(1 1 1), the H_3C—H bond is stretched while the H locates closer to surface oxygen. For both surfaces, H_3C—H bond cleavage and formation of the respective H—O_{surf} bonds are not yet completed in TS.

The geometries of both pTS and TS are shown in the supplementary information (Figs. S1 and S2).

Supplementary data associated with this article can be found, in the online version, at https://doi.org/10.1016/j.apsusc.2018.07.090.

We also performed these calculations using the vdW-DF functional, to assess the role of van der Waals forces in stabilizing methane-surface interactions. As expected, accounting for dispersion forces results in an increase of methane molecular adsorption energy. CH_4 interacts with metal cations and O sites with an adsorption energy of −0.12 eV for both the CeO_2(1 1 1) and $Ce_{0.963}Pr_{0.037}O_2$(1 1 1) surfaces. In all cases, the CH_4 molecule locates at 2–3 Å of the surface ion, similarly as predicted by PBE + U calculations. Also, the first layers of the surface undergo some relaxation with the vdW-DF approach, independently of the presence of methane. The top oxygen and cation layers show inward relaxation of 1.45% and 0.90%, respectively. These calculations evidence that, in both CeO_2(1 1 1) and $Ce_{0.963}Pr_{0.037}O_2$(1 1 1) surfaces, methane molecular adsorption is governed by weak dispersion forces. Additionally, we computed the pseudo-transition state energy with the vdW-DF functional. The calculation of ΔE[pTS] resulted in 0.98 eV for CeO_2(1 1 1) surface and 0.14 eV for $Ce_{0.963}Pr_{0.037}O_2$(1 1 1). For both surfaces, inclusion of vdW forces marginally improves the energy of methane molecular interactions (−0.12 eV) while the pTS stabilizes only in 0.02 eV. Thus, the energy differences between molecular adsorption of methane and the pTS state employing the vdW-DF functional are 0.26 eV for the $Ce_{0.963}Pr_{0.037}O_2$(1 1 1) surface and 1.10 eV for the CeO_2(1 1 1).

The geometry of TS would also be affected by vdW forces. Although CI-NEB calculations were not performed with the vdW correction, one might speculate about the TS by inspecting the configurations obtained from PBE + U calculations. For CeO_2(1 1 1), we note that the H—O_{surf} distance in TS (0.98 Å) is the same that in the pTS and H_3C—H distances are stretched over 2 Å in both states (Fig. S1); hydrogen bonding to O_{surf} is governing these interactions and no significant difference between PBE + U and vdW values for the energy transition state would be expected. Regarding $Ce_{0.963}Pr_{0.037}O_2$(1 1 1), Fig. S2 shows that the H—O_{surf} distance in the TS (1.34 Å) is longer than that in the pTS (0.98 Å) and the H_3C—H distance (1.24 Å) is only slightly elongated respect to CH_4 (1.10 Å); electrostatic interactions are still important in the TS and we would expect a difference between PBE + U and vdW energy values like that in methane molecular adsorption.

Next, to achieve a better understanding of first methane reaction step we analyzed electron occupancy, Bader charge and projected density of states (PDOS) of significant ions in the pTS for both surfaces.

Cerium cations in the stoichiometric CeO_2(1 1 1) surface are known to adopt a tetravalent oxidation state (Ce^{4+}) with unoccupied 4f orbitals (zero electrons). Accordingly, Bader calculations indicate a charge of 9.60 electrons and a magnetic moment of 0 μB for Ce^{4+} cations. In the $Ce_{0.963}Pr_{0.037}O_2$(1 1 1) surface, the Pr dopant adopts the same (4+) oxidation state than Ce cations. When computing the electron occupancy of 4f states, we verify that the Ce cations remains as Ce^{4+}, that is, all 4f orbitals are unoccupied. On the other hand, Pr(4f) states have an electron occupancy of 1.89 electrons, like that calculated for the $Ce_{0.9688}Pr_{0.0312}O_2$ bulk structure [24] and in line with the values of 1.5–1.6 electrons reported for PrO_2 [72,73]. Likewise, Bader charge is 9.60 for Ce and 10.69 for Pr; and spin magnetization results in 0 μB and 1.2 μB, respectively.

During methane dehydrogenation on the CeO_2(1 1 1) surface, hydrogen adsorption on-top of surface oxygen results in the reduction of one of the three neighboring cerium atoms, suggesting a homolytic cleavage of the first C—H bond. This result agrees with previous findings by Knapp and Ziegler [19]. On the $Ce_{0.963}Pr_{0.037}O_2$(1 1 1) surface, upon methane dissociation and hydrogen adsorption, the Pr cation is reduced. Bader charge increases from 10.69 to 10.89 electrons. A similar increase in the Pr charge was computed upon formation of an oxygen vacancy [32]. Fig. 3 illustrates the proposed electron transfer mechanism for this reaction step.

Likewise, spin magnetization analysis for the Pr cation confirms the $Pr^{4+} \rightarrow Pr^{3+}$ transition, as indicated by the increase in magnetic moment from 1.2 to 2.0 μB. Moreover, carbon shows a magnetic moment of 1.0 μB, due to the unpaired 2p electron present in the methyl radical. Fig. 4 shows the spin isosurface for this slab.

Thus, Bader charge and spin magnetization analyses also evidence a promoting role of Pr in activating the methane molecule on the $Ce_{0.963}Pr_{0.037}O_2$(1 1 1) surface; which can be ascribed to occupation of a localized Pr(4f) orbital.

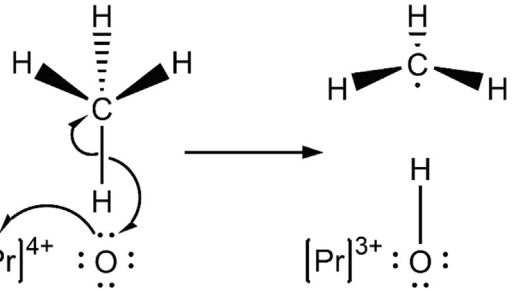

Fig. 3. Arrow pushing diagram for CH_4 activation and H adsorption on the $Ce_{0.963}Pr_{0.037}O_2$(1 1 1) surface.

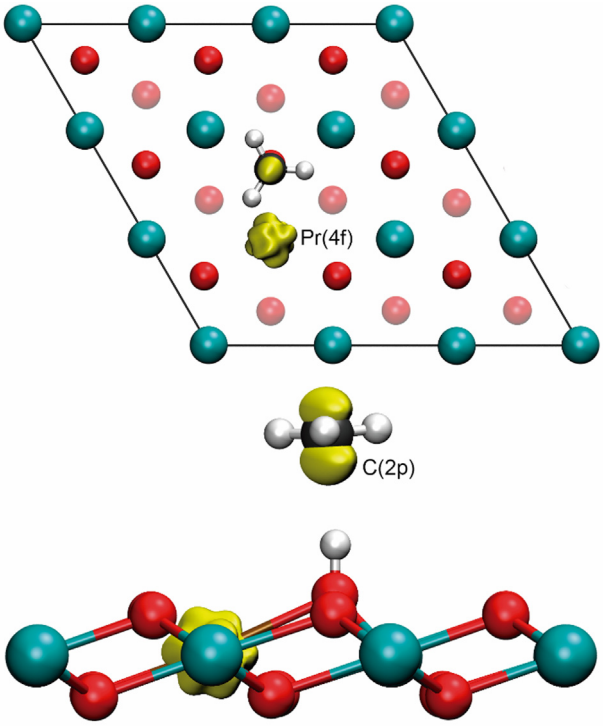

Fig. 4. Methane dehydrogenation on the $Ce_{0.963}Pr_{0.037}O_2(1\,1\,1)$ surface. Spin polarization surface at a 0.05 e/Å^3 isovalue for C(2p) and Pr(4f) orbitals. Positive and negative values are indicated in yellow and purple, respectively.

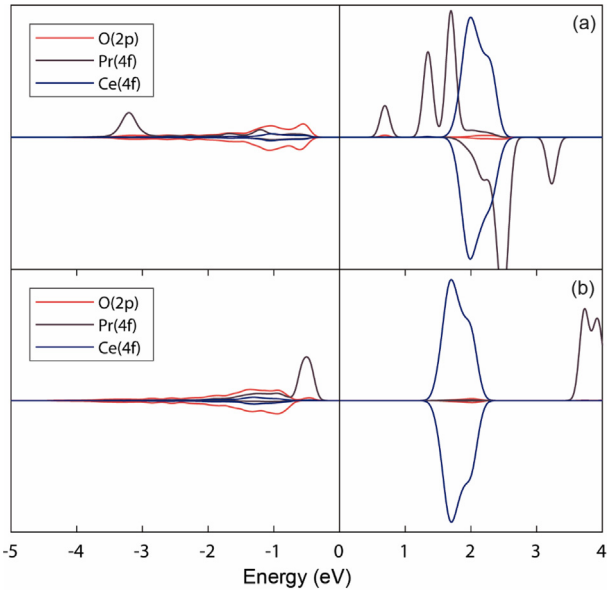

Fig. 5. Projected density of states (PDOS) on $Ce_{0.963}Pr_{0.037}O_2$ slab. (a) Stoichiometric $Ce_{0.963}Pr_{0.037}O_2(1\,1\,1)$ surface. (b) Methane pseudo-transition state.

In a previous work, we reported preferential reduction of Pr upon oxygen vacancy formation, which was explained in terms of the availability of its unoccupied 4f states [28]. This can be inferred from the projected density of the states on Ce(4f) and Pr(4f) orbitals in the $Ce_{0.963}Pr_{0.037}O_2(1\,1\,1)$ surface (Fig. 5a).

Fig. 5a shows the valence band extending between −4.25 and −0.25 eV, which consists mainly of the O(2p) states and the occupied Pr(4f) orbital, with some Ce(4f) contribution. The empty Ce(4f) states localize at 2 eV, in the gap between the valence and conduction bands. The unoccupied Pr(4f) orbitals running from 0.50 to 1.75 eV, were identified as metal-induced states. The energy gap between the top of the valence-band and the bottom of the first empty Pr(4f) peak is only 0.75 eV, suggesting that Pr(4f) states are more readily available to receive electron density than Ce(4f) states. Thus, the Pr dopant would favor reduction processes on the ceria surface. Indeed, after hydrogen adsorption on the $Ce_{0.963}Pr_{0.037}O_2(1\,1\,1)$ surface, another Pr(4f) state becomes partially occupied and moves 0.50 eV below the Fermi level as shown by the spin-up PDOS curve (Fig. 5b).

3.2. Mitigated promoting effect of the Pr^{3+} cation

As previously discussed, praseodymium's promoting effect for methane activation appears to be linked to a modification in the electronic structure of ceria. Namely, the dopant introduces metal–induced unoccupied Pr(4f) gap states located closer to the valence band than Ce (4f) states. Upon methane activation on the Pr-doped surface, the Pr cation is reduced to Pr^{3+} and its remaining unoccupied Pr(4f) states are moved to a higher energy. This suggests that the C—H bond breaking promoting effect of Pr may be counteracted by its reduction. We studied the next reaction step to test this hypothesis.

After methane activation on ceria, the methyl radical adsorbs on a surface oxygen site and undergoes subsequent oxidation [19,69,70]. We computed the interaction of a CH_3 radical on O8, the nearest neighbor of the O4 anion where the first H atom was adsorbed (Fig. 6a).

On the H − $CeO_2(1\,1\,1)$ system, the CH_3 adsorption energy value is −2.30 eV, similar to the −2.50 eV reported by Knapp and Ziegler [19]. CH_3 locates 1.43 Å above O8, leading to reduction of another surface Ce cation; which shows an increase in its Bader charge from 9.60 to 9.87 electrons. Notably, for the H − $Ce_{0.963}Pr_{0.037}O_2(1\,1\,1)$ system (note that its single Pr cation was reduced to Pr^{3+}) we calculate the CH_3 adsorption value in −2.33 eV. Once again, CH_3 locates 1.43 Å above O8 and a Ce cation is reduced.

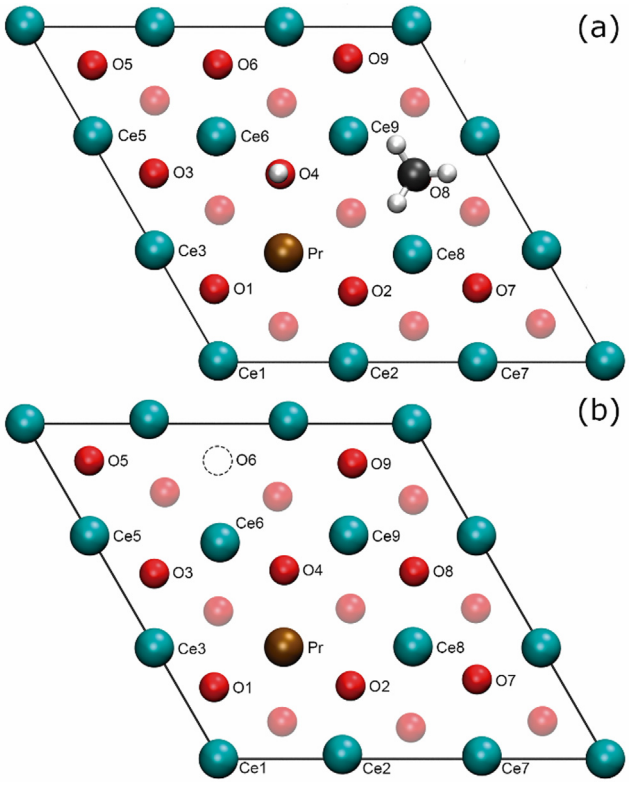

Fig. 6. (a) CH_3 and H fragments adsorbed on the $Ce_{0.963}Pr_{0.037}O_2(1\,1\,1)$ surface. (b) O6-deficient $Ce_{0.963}Pr_{0.037}O_2(1\,1\,1)$ surface. The dashed line circle shows the location of the oxygen vacancy.

These calculations show that CH_3 adsorption energy in the Pr-doped system, with the dopant cation in the Pr^{3+} state, is similar to that in the undoped H − CeO_2(1 1 1) system; supporting our hypothesis of a mitigated promoting effect of Pr^{3+} cations. To further investigate this compensation of the promoting effect, we also examined methane interactions with a $Ce_{0.963}Pr_{0.037}O_{2-x}$(1 1 1) surface in which the Pr dopant was reduced by removing the O6 anion (Fig. 6b). Indeed, the electron pair left behind by formation of the oxygen vacancy lead to reduction of the Pr dopant and a Ce cation, due to occupation of one of their 4f states. Accordingly, Bader charge analysis shows 9.94 electrons for Ce8 and 10.89 electrons for Pr, and spin magnetizations of 1.0 μB and 2.0 μB, respectively. These values correspond to Ce^{3+} and Pr^{3+} cations.

Our calculations indicated no significant methane molecule interactions on the O–deficient $Ce_{0.963}Pr_{0.037}O_{2-x}$(1 1 1) surface. The CH_4 molecule locates 2.46 Å above the O4 anion with nearly-null adsorption energy, like on stoichiometric $Ce_{0.963}Pr_{0.037}O_2$(1 1 1) and CeO_2(1 1 1) surfaces.

For the O6-deficient surface, we calculated a pseudo-transition state energy (ΔE[pTS]) of 1.02 eV. This value is virtually the same that in the CeO_2(1 1 1) surface but higher than in the stoichiometric Pr-doped surface. Therefore, our results confirm that the promoting effect of Pr doping is counteracted when Pr is reduced to Pr^{3+}.

Our findings could be better understood by examining the DOS curve for the O6-deficient $Ce_{0.963}Pr_{0.037}O_{2-x}$(1 1 1) surface (Fig. 7). The curve shows Pr(4f) and Ce8(4f) occupied states located 1.14 eV and 0.45 eV below the Fermi level respectively. Further reduction of this surface would require occupation of the empty Ce(4f) states located at 1.13 eV. This means that, in our slab, the promoting effect of the Pr cation is lost when it is reduced by oxygen vacancy formation or hydrogen adsorption.

For practical purposes, oxygen vacancies formation and hydrogen or methyl adsorption could counteract the positive effect of Pr^{4+} for promoting the activation of new methane molecules. Thus, a fast renewal of surface oxygen is important to ensure the availability of praseodymium in the Pr^{4+} oxidation state.

3.3. CH_4-TPR of $Ce_{0.95}Pr_{0.05}O_2$ and CeO_2 samples

Ceria and Pr-doped ceria samples reduction by methane may be considered to proceed as follows [74]: $CH_4 \rightarrow CH_{4-x}^{*} + xH^{*}$. The adsorbed H atoms can recombine and leave the surface either as H_2 or H_2O. Desorption of H_2O requires oxygen from the ceria surface. After successive C−H bonds cleavages, adsorbed carbon can be released as CO with concomitant oxygen vacancy formation. The CO species can be further oxidized to CO_2 generating additional oxygen vacancies. Alternatively, the CH^{*} fragments can oxidize to HCO^{*} intermediates, which can also desorb as CO_2 [75]. Therefore, partial and total methane oxidation products (H_2, CO, H_2O and CO_2) could be expected at the reactor outlet.

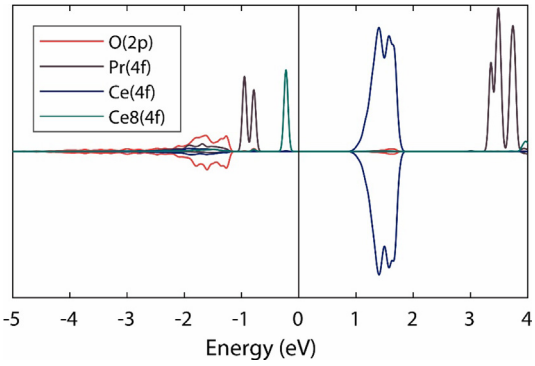

Fig. 7. Projected density of states (PDOS) for the O6-deficient $Ce_{0.963}Pr_{0.037}O_2$(1 1 1) surface.

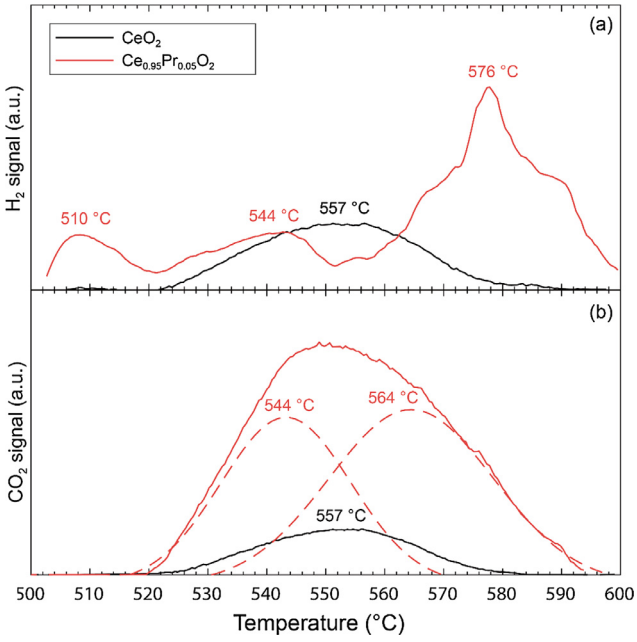

Fig. 8. CH_4-TPR profiles for the $Ce_{0.95}Pr_{0.05}O_2$ and CeO_2 samples calcined at 900 °C. (a) H_2. (b) CO_2.

Fig. 8 shows the CH_4-TPR profiles obtained at reaction temperatures in the range 500–600 °C. These curves are the result of repeated measurements. Furthermore, different heating rates led to similar downshift in products desorption temperature for all CH_4-TPR experiments. In these experiments, we used samples calcined at 900 °C to discard any textural transformation. For both the CeO_2 and $Ce_{0.95}Pr_{0.05}O_2$ samples, only CO_2, H_2 and H_2O were detected at the reactor outlet, with negligible CO production.

Regarding methane reactions on CeO_2, the work of Trovarelli [17] has shown that methane activation by splitting the C−H bond occurs on surface lattice-oxygen anions with formation of stabilized surface OH species. This review also indicates that methane adsorption on surface coordinately unsaturated oxygen species, leads to activation of the C−H bond at low temperature with formation of formates. These species evolve decomposing to surface carbonates, and finally desorb as CO and H_2O at higher temperatures [17]. On the other hand, CH_4-TPR experiments have shown that, below 650 °C, the only products from methane reaction with undoped ceria catalyst are CO_2 and H_2O [76], whereas H_2 and CO products have been obtained from reaction of methane with CeO_2 at temperatures higher than 700 °C [77]. Overall, CO, CO_2, H_2 and H_2O are released depending on the experimental conditions. Herein, Fig. 8 shows that ceria reduction begins at 523 °C, and that H_2 and CO_2 production occurs simultaneously in a single event.

Concerning methane reaction on Pr-doped ceria, it is worth noting that H_2 and CO_2 production in the $Ce_{0.95}Pr_{0.05}O_2$ sample is 2.80–2.90 times higher than in the undoped CeO_2 sample (see Fig. 8a and b). The increase in the amount of CO_2 released in the $Ce_{0.95}Pr_{0.05}O_2$ sample could be ascribed to its improved oxygen mobility due to Pr addition into the lattice. Facilitated oxygen donation of Pr-doped ceria samples has been previously reported from experimental measurements (oxygen storage capacity experiments, Raman spectroscopy, and X-ray photoelectron spectroscopy) and DFT calculations [31]. We measured an oxygen storage capacity (OSC) for our samples of 19 μmolCO_2/g for CeO_2 and 56 μmolCO_2/g for $Ce_{0.95}Pr_{0.05}O_2$, which gives a OSC_{doped}/$OSC_{undoped}$ ratio of 2.95. Thus, the increased H_2 and CO_2 production from the $Ce_{0.95}Pr_{0.05}O_2$ sample might be correlated with its superior OSC. The surface anion vacancies generated by CO_2 release could be

easily refilled with lattice oxygen due to the sample's enhanced OSC; resulting in continuous availability of surface active O-sites to adsorb hydrogen and methyl fragments, and therefore in higher H_2 and CO_2 production.

The H_2 profile shown in Fig. 8a evidences that Pr-doped ceria promotes the C—H bond cleavage in methane. In the $Ce_{0.95}Pr_{0.05}O_2$ sample, H_2 desorption begins at 500 °C, whereas in the CeO_2 sample the desorption temperature is higher by 23 °C. This result confirms that Pr facilitates CH_4 activation, and it is in line with the lower energy barrier calculated for the first C—H bond cleavage on Pr-doped CeO_2.

The H_2 profiles (Fig. 8a) for the Pr-doped sample exhibit three maximums at 510, 545, and 576 °C; as opposed to the single maximum in pure CeO_2 at 557 °C. It has been well documented that methane activation on CeO_2 is limited by the high-energy barrier of the first C—H bond cleavage [69]. Therefore, if the temperature is enough for methane activation, the following steps would also rapidly occur. Accordingly, the H_2 profile of CeO_2 sample shows only one peak, which would include hydrogen from the H_3C—H bond cleavage but also from dehydrogenation of the CH_3^*, CH_2^*, and CH^* fragments. Besides, the CO_2 peak also appears around 557 °C (Fig. 8b) which proves that methane undergoes quick dehydrogenation and oxidation after the activation step.

Instead, in the $Ce_{0.95}Pr_{0.05}O_2$ sample the first maximum of the H_2 profile at 510 °C is not accompanied by CO or CO_2, suggesting that adsorbed CH_x fragments would not be completely dehydrogenated an oxidized at this low temperature. Indeed, complete methane oxidation to CO_2 is observed starting from 520 °C. We speculate that methane activation could mitigate the promoting effect of Pr by electron occupancy of metal-induced 4f states (see Section 3.2) and so, subsequent CH_x dehydrogenations would become kinetically relevant. In this sense, Knapp reported that dehydrogenation of adsorbed CH_3 fragments involve an energy barrier of 1.30 eV [19], which is higher than the methane activation barrier that we calculated on the Pr-doped CeO_2(1 1 1) surface (0.82 eV). Consequently, CO_2 is released at higher temperatures than that of the first H_2 peak.

The H_2 profile also shows peaks with maximums at 545 and 576 °C, which are enveloped by the CO_2 curve extending from 520 to 600 °C. Besides, the CO_2 curve profile can be deconvoluted in two peaks concurrent with the H_2 maximums. Therefore, the second and third H_2 peaks could be associated to dehydrogenation steps that lead to a differentiated release of CO_2, involving different mechanisms such as formation of intermediate species or methane activation on different surface sites on the Pr-doped ceria sample.

Overall, the DFT calculations are well validated by the CH_4-TPR experiments. Our theoretical findings provide a comprehensive fundamental understanding of the promoting effect of praseodymium in methane activation and oxidation reactions on ceria-based supports; which can be associated with the dopant ability to form Pr^{4+}/Pr^{3+} redox couples. Both the theoretical and experimental results evidence that methane activation is boosted by doping ceria with low concentrations of Pr and the promoting effect is mitigated with progressive reduction of solids.

4. Conclusions

Density functional theory (DFT) calculations performed on a low-doped Pr-CeO_2(1 1 1) slab allowed us to elucidate the effect of Pr doping for methane interactions with this surface.

Methane activation occurs through a rebound mechanism, in which hydrogen atoms adsorb on a surface oxygen atom and methyl radicals are released to the gas phase. On the $Ce_{0.963}Pr_{0.037}O_2$(1 1 1) surface, the energy barrier for this step is lowered by 0.48 eV compared to the undoped CeO_2(1 1 1) surface, indicating that methane activation is facilitated by the Pr dopant. On the stoichiometric surface, the dopant adopts a Pr^{4+} oxidation state. Metal-induced Pr(4f) gap states are closer to the Fermi level than Ce(4f) states, and therefore more readily available to receive an electron from hydrogen that bounds to surface lattice oxygen. Upon hydrogen adsorption, a Pr(4f) state is occupied with one electron and the remaining empty states move to higher energies. The promoting effect of Pr^{4+} for methane activation, or other reaction steps involving electron transfer to the surface, is mitigated when praseodymium is reduced to Pr^{3+}.

Methane temperature-programed reduction (CH_4-TPR) experiments conducted in $Ce_{0.95}Pr_{0.05}O_2$ and CeO_2 samples, at temperatures between 500 and 600 °C, validate the theoretical results. On the $Ce_{0.95}Pr_{0.05}O_2$ sample, the production of H_2 begins at 500 °C, 23 °C lower than that on CeO_2, revealing the promoting effect of Pr for methane activation. This is in line with the lower energy barrier computed for the first C—H bond cleavage on the $Ce_{0.963}Pr_{0.037}O_2$(1 1 1) surface. Besides, H_2 and CO_2 production correlates well with the increase in OSC of the Pr-doped sample.

In summary, our findings allow us to anticipate a superior performance of low-doped Pr-CeO_2 based-catalyst for syngas and hydrogen production by methane reforming at low temperatures.

Acknowledgments

This work was supported by Universidad de Buenos Aires (20020150100095BA) and ANPCyT (PICT-2015-2135). Agustín Salcedo and Ignacio Iglesias thank FIUBA for the Peruilh doctoral fellowship.

References

[1] R. Chaubey, S. Sahu, O.O. James, S. Maity, Renew. Sustain. Energy Rev. 23 (2013) 443–462.
[2] M. Balat, Int. J. Hydrogen Energy 33 (2008) 4013–4029.
[3] H. Balat, E. Kırtay, Int. J. Hydrogen Energy 35 (2010) 7416–7426.
[4] H. Larsen, R. Feidenhans, L.S. Petersen,, Risø energy report 3: hydrogen and its competitors, Renew. Sustain. Energy Rev. (2004).
[5] S. Grierson, V. Strezov, G. Ellem, R. Mcgregor, J. Herbertson, J. Anal. Appl. Pyrol. 85 (2009) 118–123.
[6] J.R. Rostrup-Nielsen, Catalysis, Springer, Berlin, Heidelberg, 1984, pp. 1–117.
[7] J.R. Rostrup-Nielsen, Catal. Today 18 (1993) 305–324.
[8] R.M. Navarro, M.A. Peña, J.L.G. Fierro, Chem. Rev. 107 (2007) 3952–3991.
[9] J. Sehested, Catal. Today 111 (2006) 103–110.
[10] K. Aasberg-Petersen, I. Dybkjær, C.V. Ovesen, N.C. Schjødt, J. Sehested, S.G. Thomsen, J. Nat. Gas Sci. Eng. 3 (2011) 423–459.
[11] A. Purnomo, S. Gallardo, L. Abella, C. Salim, H. Hinode, React. Kinet. Catal. Lett. 95 (2008) 213–220.
[12] S. Xu, X. Yan, X. Wang, Fuel 85 (2006) 2243–2247.
[13] F.B. Passos, E.R. de Oliveira, L.V. Mattos, F.B. Noronha, Catal. Today 101 (2005) 23–30.
[14] T.J. Huang, C.H. Wang, Chem. Eng. J. 132 (2007) 97–103.
[15] C. Zhang, A. Michaelides, D.A. King, S.J. Jenkins, Phys. Rev. B 79 (2009) 75433.
[16] C.T. Campbell, Science 309 (2005) 713–714.
[17] A. Trovarelli, Catal. Rev. Sci. Eng. 38 (1996) 439–520.
[18] P. Mars, D.W. van Krevelen, Chem. Eng. Sci. 3 (1954) 41–59.
[19] D. Knapp, T. Ziegler, J. Phys. Chem. C 112 (2008) 17311–17318.
[20] D.R. Mullins, Surf. Sci. Rep. 70 (2015) 42–85.
[21] Z. Yang, Y. Wei, Z. Fu, Z. Lu, K. Hermansson, Surf. Sci. 602 (2008) 1199–1206.
[22] E.W. McFarland, H. Metiu, Chem. Rev. 113 (2013) 4391–4427.
[23] D.A. Andersson, S.I. Simak, B. Johansson, I.A. Abrikosov, N.V. Skorodumova, Phys. Rev. B - Condens. Matter. Mater. Phys. 75 (2007) 4–9.
[24] Y. Tang, H. Zhang, L. Cui, C. Ouyang, S. Shi, W. Tang, H. Li, J.-S. Lee, L. Chen, Phys. Rev. B - Condens. Matter Mater. Phys. 82 (2010) 125104.
[25] D. García Pintos, A. Juan, B. Irigoyen, Int. J. Hydrogen Energy 37 (2012) 14937–14944.
[26] Z. Yang, T.K. Woo, K. Hermansson, J. Chem. Phys. 124 (2006) 224704.
[27] R. Chiba, T. Komatsu, H. Orui, H. Taguchi, K. Nozawa, H. Arai, Electrochem. Solid-State Lett. 12 (2009) B69.
[28] P.P. Dholabhai, J.B. Adams, P. Crozier, R. Sharma, J. Chem. Phys. 132 (2010) 94104.
[29] A. Gupta, U.V. Waghmare, M.S. Hegde, Chem. Mater. 22 (2010) 5184–5198.
[30] E. Poggio-Fraccari, F. Mariño, M. Laborde, G. Baronetti, Appl. Catal. A: Gen. 460–461 (2013) 15–20.
[31] E. Poggio-Fraccari, B. Irigoyen, G. Baronetti, F. Mariño, Appl. Catal. A: Gen. 485 (2014) 123–132.
[32] B. Milberg, A. Juan, B. Irigoyen, Appl. Surf. Sci. 401 (2017) 206–217.
[33] K. Ahn, D.S. Yoo, D.H. Prasad, H.W. Lee, Y.C. Chung, J.H. Lee, Chem. Mater. 24 (2012) 4261–4267.
[34] A. Kaddouri, B. Béguin, Catal. Commun. 46 (2014) 22–27.
[35] G. Kresse, J. Furthmüller, Phys. Rev. B 54 (1996) 11169–11186.

[36] G. Kresse, J. Hafner, Phys. Rev. B 47 (1993) 558–561.
[37] J.P. Perdew, K. Burke, M. Ernzerhof, Phys. Rev. Lett. 77 (1996) 3865–3868.
[38] G. Kresse, Phys. Rev. B. 59 (1999) 1758–1775.
[39] P.E. Blöchl, Phys. Rev. B 50 (1994) 17953–17979.
[40] H.J. Monkhorst, J.D. Pack, Phys. Rev. B 13 (1976) 5188–5192.
[41] M. Nolan, S.C. Parker, G.W. Watson, Surf. Sci. 595 (2005) 223–232.
[42] M.V. Ganduglia-Pirovano, A. Hofmann, J. Sauer, Surf. Sci. Rep. 62 (2007) 219–270.
[43] C. Loschen, J. Carrasco, K.M. Neyman, F. Illas, Phys. Rev. B - Condens. Matter Mater. Phys. 75 (2007) 1–8.
[44] N.V. Skorodumova, S.I. Simak, B.I. Lundqvist, I.A. Abrikosov, B. Johansson, Phys. Rev. Lett. 89 (2002) 166601.
[45] M.V. Ganduglia-Pirovano, J.L.F. Da Silva, J. Sauer, Phys. Rev. Lett. 102 (2009) 26101.
[46] S.L. Dudarev, G.A. Botton, S.Y. Savrasov, C.J. Humphreys, A.P. Sutton, Phys. Rev. B. 57 (1998) 1505–1509.
[47] C.W.M. Castleton, J. Kullgren, K. Hermansson, J. Chem. Phys. 127 (2007) 244704.
[48] M. Nolan, S.C. Parker, G.W. Watson, J. Phys. Chem. B 110 (2006) 2256–2262.
[49] M. Nolan, G.W. Watson, J. Phys. Chem. B 110 (2006) 16600–16606.
[50] M. Dion, H. Rydberg, E. Schröder, D.C. Langreth, B.I. Lundqvist, Phys. Rev. Lett. 92 (2004) 246401.
[51] D. Fernández-Torre, K. Kośmider, J. Carrasco, M.V. Ganduglia-Pirovano, R. Pérez, J. Phys. Chem. C 116 (2012) 13584–13593.
[52] G. Román-Pérez, J.M. Soler, Phys. Rev. Lett. 103 (2009) 96102.
[53] J. Klimeš, D.R. Bowler, A. Michaelides, Phys. Rev. B 83 (2011) 195131.
[54] G. Henkelman, B.P. Uberuaga, H. Jónsson, J. Chem. Phys. 113 (2000) 9901–9904.
[55] R.F.W. Bader, Chem. Rev. 91 (1991) 893–928.
[56] G. Henkelman, A. Arnaldsson, H. Jónsson, Comput. Mater. Sci. 36 (2006) 354–360.
[57] L. Eyring, The binary rare earth oxides, in: K.A. Gschneidner, L. Eyring (Eds.), Handbook on the Physics and Chemistry of Rare Earths, Elsevier, Amsterdam, 1979, pp. 337–399.
[58] M.-F. Luo, Z.-L. Yan, L.-Y. Jin, J. Mol. Catal. A: Chem. 260 (2006) 157–162.
[59] B.M. Reddy, G. Thrimurthulu, L. Katta, Y. Yamada, S. Park, J. Phys. Chem. C 113 (2009) 15882–15890.
[60] Z. Song, W. Liu, H. Nishiguchi, A. Takami, K. Nagaoka, Y. Takita, Appl. Catal. A: Gen. 329 (2007) 86–92.
[61] R.D. Shannon, Acta Crystallogr. Sect. A 32 (1976) 751–767.
[62] S. Fabris, G. Vicario, G. Balducci, S. de Gironcoli, S. Baroni, J. Phys. Chem. B 109 (2005) 22860–22867.
[63] M. Nolan, S. Grigoleit, D.C. Sayle, S.C. Parker, G.W. Watson, Surf. Sci. 576 (2005) 217–229.
[64] N.V. Skorodumova, M. Baudin, K. Hermansson, Phys. Rev. B 69 (2004) 1–8.
[65] M. Jobbágy, F. Mariño, B. Schönbrod, G. Baronetti, M. Laborde, Chem. Mater. 18 (2006) 1945–1950.
[66] E. Poggio, M. Jobbágy, M. Moreno, M. Laborde, F. Mariño, G. Baronetti, Int. J. Hydrogen Energy 36 (2011) 15899–15905.
[67] H.C. Yao, Y.F. Yu Yao, J. Catal. 86 (1984) 254–265.
[68] I. Iglesias, G. Baronetti, F. Mariño, Solid State Ionics 309 (2017) 123–129.
[69] M.D. Krcha, A.D. Mayernick, M.J. Janik, J. Catal. 293 (2012) 103–115.
[70] M. Fronzi, S. Piccinin, B. Delley, E. Traversa, C. Stampfl, RSC Adv. 4 (2014) 12245–12251.
[71] R. Horn, R. Schlögl, Catal. Lett. 145 (2015) 23–39.
[72] A. Bianconi, A. Kotani, K. Okada, R. Giorgi, A. Gargano, A. Marcelli, T. Miyahara, Phys. Rev. B 38 (1988) 3433–3437.
[73] H. Ogasawara, A. Kotani, R. Potze, G.A. Sawatzky, B.T. Thole, Phys. Rev. B 44 (1991) 5465–5469.
[74] T.-J. Huang, H.-J. Lin, T.-C. Yu, Catal. Lett. 105 (2005) 239–247.
[75] A.D. Mayernick, M.J. Janik, J. Catal. 278 (2011) 16–25.
[76] Lj. Kundakovic, M. Flytzani-Stephanopoulos, J. Catal. 179 (1998) 203–221.
[77] K. Otsuka, E. Sunada, T. Ushiyama, I. Yamanaka, Stud. Surf. Sci. Catal. 107 (1997) 531–536.